Origin of the anomalous Hall effect at the magnetic insulator/heavy metals interface

Sajid Husain, Nicholas Figueiredo-Prestes, Olivier Fayet, Sophie Collin, Florian Godel, Eric Jacquet, Nicolas Reyren, Henri Jaffrès, Jean-Marie George

Applied Physics Letters

Origin of the anomalous Hall effect at the magnetic insulator/heavy metals interface

Cite as: Appl. Phys. Lett. **122**, 062403 (2023); https://doi.org/10.1063/5.0132895
Submitted: 31 October 2022 • Accepted: 23 January 2023 • Published Online: 08 February 2023

Sajid Husain, Nicholas Figueiredo-Prestes, Olivier Fayet, et al.

Applied Physics Letters ARTICLE scitation.org/journal/apl

Origin of the anomalous Hall effect at the magnetic insulator/heavy metals interface

Cite as: Appl. Phys. Lett. **122**, 062403 (2023); doi: 10.1063/5.0132895
Submitted: 31 October 2022 · Accepted: 23 January 2023 ·
Published Online: 8 February 2023

Sajid Husain,[a),b)] Nicholas Figueiredo-Prestes, Olivier Fayet, Sophie Collin, Florian Godel, Eric Jacquet, Nicolas Reyren, Henri Jaffrès,[c)] and Jean-Marie George[a)]

AFFILIATIONS

Unité Mixte de Physique, CNRS, Thales, Université Paris-Saclay, 91767 Palaiseau, France

[a)]**Authors to whom correspondence should be addressed:** shusain@lbl.gov and jeanmarie.george@cnrs-thales.fr
[b)]**Present address:** Material Physics Division, Lawrence Berkeley National Laboratory, Berkeley, California 94720, USA.
[c)]**Electronic mail:** henri.jaffres@cnrs-thales.fr

ABSTRACT

Ferrimagnetic insulators (FIMIs) are considered to be promising candidates in spin–orbit torque (SOT) devices due to their ability to propagate a spin current by magnons without Ohmic losses owing to the absence of electronic scattering. Moreover, any electrical current shunt is avoided in magnetic insulating materials. On the other hand, SOT-induced magnetization switching is generally measured through the anomalous Hall effect (AHE) in FIMI/heavy metal (HM) systems. However, the origin of AHE in FIMI/HM remains elusive since charges flow only in the HM. Here, we experimentally demonstrate that the AHE has the same origin as the spin Hall magnetoresistance (SMR). To this end, we have studied two bilayer heterostructures, $Tm_3Fe_5O_{12}$(TmIG)/W and TmIG/Pt, where we ensure opposite spin Hall effect (SHE) signs for two heavy metals (W and Pt). The magnitudes of AHE and SMR are found to be larger for TmIG/W than TmIG/Pt. We have also evidenced the identical polarity of AHE hysteresis in both systems revealing a square dependency on the spin Hall angle whereas the current-induced magnetization switching polarity in TmIG/W is opposite to that of TmIG/Pt as expected for opposite spin Hall angle signs. Our results establish that the AHE and the spin-Hall magnetoresistance in TmIG insulating ferromagnets and heavy metal bilayers originate from the same mechanism.

Spin current defined as a flow of angular momentum with no net charge[1] makes spintronic devices very efficient as the Joule heating is, thus, minimized.[2] This becomes more suitable if the ferromagnet (FM) is an insulator,[2–4] because it avoids any electrical current shunt through the FM material. For the spin–orbit torque (SOT) based magnetization switching operations,[5–7] an electrical charge injected into heavy metals (HMs) gets polarized owing to the spin Hall effect (SHE)[8] or/and the Rashba-Edelstein effect (REE)[9,10] with the result that spins accumulate at the interface. Followed by an angular momentum transfer, the spin accumulation is able to excite and even reverse a magnetic state or to move domain walls.[11] The SOT-induced magnetization switching in ferrimagnetic insulator (FIMI)/HM systems is generally measured through the change in the anomalous Hall effect (AHE) resistance.[12] Though the origin of AHE in FIMI/HM remains elusive, the charge current flows only in HM and the ferrimagnetic insulator (FIMI) does not allow any electrical conduction. Therefore, AHE/SHE[13] contributions and anomalous Hall magnetoresistance[14] from the FIMI itself may then be neglected. Several origins of the AHE-like signal in FIMI/HM bilayers (hereafter called spin-Hall AHE or simply called AHE in this paper) have been discussed in the literature, which invoke proximity effect,[15] interfacial spin–orbit assisted electron scattering,[16–18] and spin Hall magnetoresistance(SMR).[12,19,20] The former appears to be due to the induced magnetization in the HM as a result of an electronic distribution among orbitals, which depends on the spin–orbit coupling (SOC), whereas the latter two effects involve spin current-driven mechanisms. In the scheme of a spin-dependent scattering mechanism of the bulk SHE current at the magnetic interface as well as in the scheme of the SHE in the bulk of the HM, the effect is coined as non-local AHE, and one can predict that its sign is determined by the sign of the spin-Hall angle (SHA).[18] This is experimentally demonstrated in Pt/$(Co/Ni)_N$ multi-layers (N is the number of repetitions), where the polarity of the AHE hysteresis derives from the sign of the SHA.[17]

In this Letter, we discuss the origin of AHE and its relationship to the SMR and to the current-induced magnetization switching in insulating magnet-based systems using materials of two opposite SHA.

In particular, among the different sources of AHE with insulators, our work clearly demonstrates the prominent role of the SMR in the current perpendicular to plane geometry over other possible mechanisms as played the spin-polarization via spin–orbit scattering at the interface for current flows in-plane in all-metallic systems.[21] In the case of FIMI/HM bilayers where the current flows only in HM, due to the SHE, polarized electrons of spin σ interact with the magnetization **M** through the local exchange interactions giving subsequent SOT. This phenomenon depends on the angle between **M** and σ, and, owing to the related change of the spin-accumulation, this results in a change in the resistance of the HM known as spin Hall magnetoresistance (SMR).[12] To discuss the interfacial spin phenomena involved at the interface between a magnetic insulator and a heavy metal, we present the experimental results involving the signature of spin accumulation/current at the interface, i.e., (i) anomalous Hall effect, (ii) angular or magnetic field dependence of SMR and anisotropic magnetoresistance (AMR), (iii) torque induced by the spin current, and (iv) magnetization reversal induced by a spin current. It will then ends with our main conclusion on the origin of the anomalous Hall effect.

For this purpose, we have prepared thulium iron garnet $Tm_3Fe_5O_{12}$ (TmIG), thin films of thickness 10 nm on a $Gd_3Ga_5O_{12}$ (GGG) substrate by off-axis magnetron sputtering. TmIG thin films were deposited at room temperature and then post-annealed at 650 °C for 4 h in molecular O_2 flow at atmospheric pressure. The heavy metal layers, either tungsten (W) or platinum (Pt), were subsequently grown (*ex situ*) on top of TmIG at room temperature by sputtering. For W, the film is capped by a thin layer of Al(2 nm) to protect W from atmospheric exposure. TmIG film surfaces were cleaned by O_2 plasma (~40 eV) before heavy metal deposition. Electronic transport measurements were performed on Hall-bar devices made of three 5-μm wide stripes (six contact geometry) patterned using optical lithography and Ar-ion beam milling. AHE, SMR, and AMR measurements were carried out using a constant dc current source. The second harmonic Hall measurements were performed with an ac current source on symmetric Hall cross-bars (of the same cross section) to extract the damping-like and field-like torques displayed below using lock-in detection techniques. For the current-induced magnetization switching measurements, current pulses with a duration of 100 μs were injected into the Hall bar. After each pulse, a small excitation of 100 μA current was applied to measure the Hall resistance.

We first characterize the TmIG samples by x-ray diffraction (XRD). Diffraction patterns of TmIG/W are shown in Fig. 1(a). Laue oscillations are visible around the peak (4 4 4) suggesting the smooth growth of TmIG on GGG. The W films are grown polycrystalline without favored orientation, as shown in the inset (grazing incident XRD patterns). The film of lower thickness W (8 nm) is expected to be

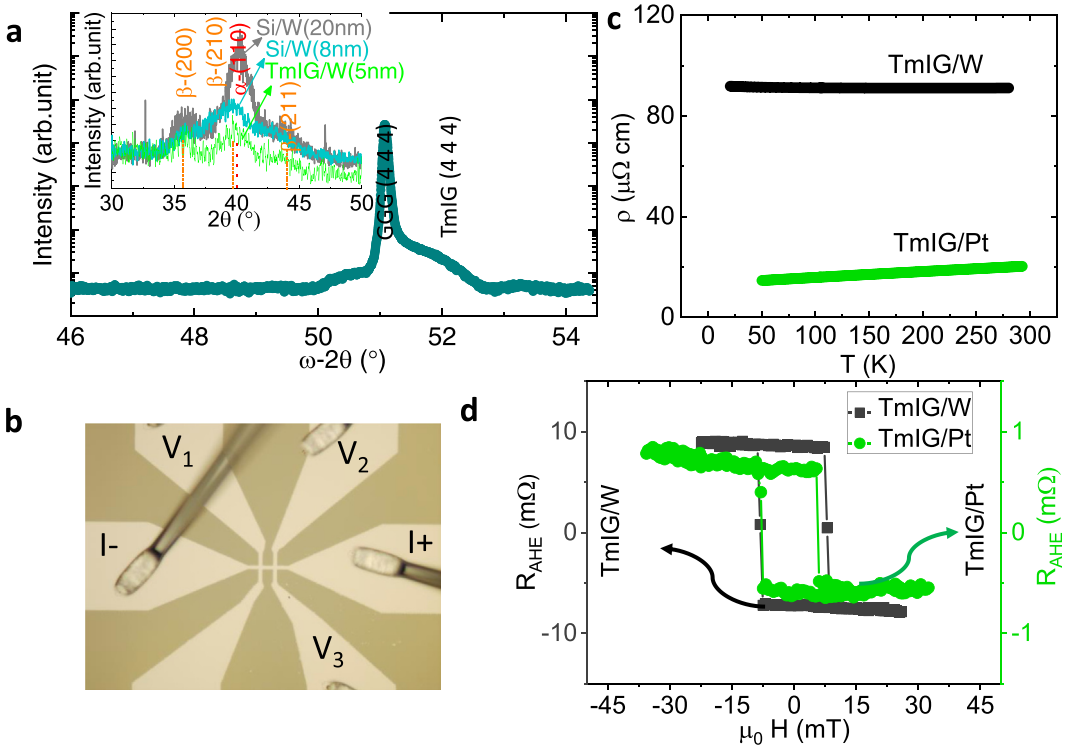

FIG. 1. (a) X-ray diffraction patterns of TmIG and W. ω-2 θ diffraction pattern corresponds to (4 4 4) reflection of TmIG and GGG. Inset: Grazing incident diffraction patterns correspond to Si/W (20 nm), Si/W (8 nm), and GGG/TmIG (10 nm)/W (5 nm). Lines are the markers corresponding to standard diffraction lines of β-W and α-W. (b) Optical image of Hall-bar along with the electrical circuit. V_1 and V_2 were used for the longitudinal resistance measurement while V_2 and V_3 used for the transverse resistance. (c) Longitudinal resistivity as a function of temperature for TmIG/W and TmIG/Pt. (d) Anomalous Hall hysteresis measured in TmIG (10 nm)/W (5 nm) (left axis) and reference sample, TmIG (10 nm)/Pt (6 nm) (right axis).

dominant with the β-W phase. We further recorded the XRD pattern on TmIG (10 nm)/W (5 nm), which also shows the dominant β-W. Since TmIG is an insulator, the resistivity measurement of W provides information about the phase of W. (α- or β-W phases have large resistivity differences.[22]) The patterned device and measurement circuit for the longitudinal and transverse resistivity are shown in Fig. 1(b). The resistivity as a function of temperature is shown in Fig. 1(c). At room temperature, it is found to be 91 $\mu\Omega$ cm close to the expected value for the dominating β-W phase.[22] On the other hand, the Pt resistivity is measured to be equal to 25 $\mu\Omega$ cm for the same film thickness. Now we come to the variation in the AHE resistance obtained by applying an out-of-plane magnetic field as shown in Fig. 1(d). Note that the magnitude of the AHE signal of TmIG/W is found to be about one order of magnitude larger than the one of TmIG/Pt. We emphasize that the polarity of the AHE hysteresis is equal in both W and Pt cases, despite the fact that Pt[23] and W[22] possess opposite spin Hall angles as already observed previously.[24] This clearly demonstrates that the magnetization hysteresis polarity has no specific dependence upon the sign of the spin Hall angle. However, the large AHE amplitude observed for the W layer used as a SHE source suggests the prominent role of the large spin current conversion as expected from W and its large spin-Hall angle.[25,26]

Before presenting the torque measurements, we review the SMR and AMR as measured using the lock-in technique at the first harmonic. We mainly present the results obtained from the W/TmIG interface since the results for Pt/TmIG have been reported elsewhere.[27]

Both the SMR and AMR are determined by measuring the longitudinal ($R_{xx} = (V_2 - V_1)/I$) and transverse ($R_{xy} = (V_2 - V_3)/I$) resistances as a function of the in-plane magnetic field or angular dependence. They are linked by the following equations:

$$R_{xx} = R_{0,xx} + \Delta R_{\mathrm{SMR}} \cos^2\varphi + \Delta R_{AMR} \cos^2\varphi\,, \tag{1}$$

$$R_{xy} = R_{0,xy} + \Delta R_{\mathrm{AHE}} \cos\theta + \frac{\Delta R_{\mathrm{SMR}}}{2} \cos^2\theta \sin 2\varphi, \tag{2}$$

where $R_{0,ij}$ is a spurious offset signal in the case of R_{xy} and the ordinary resistance in the case of R_{xx}. θ and φ are the normal and azimuthal angles, respectively. ΔR_{SMR} and ΔR_{AHE} represent the SMR and AHE resistance amplitudes, respectively, which depend on several factors such as the spin mixing conductance ($G_{\uparrow\downarrow}$: $G^R_{\uparrow\downarrow}$ and $G^I_{\uparrow\downarrow}$ are the respective real and imaginary parts of the spin-mixing conductance, respectively), spin Hall angle (θ_{SH}), HM layer thickness (t_{W}), spin diffusion length (λ_s), and spin-resistance of HM (r_s^{W}). We have[19,28]

$$\begin{aligned}
\frac{\Delta R_{\mathrm{SMR}}}{R} &= \theta_{\mathrm{SH}}^2 \frac{\lambda_s}{t_{\mathrm{W}}} \frac{2G^R_{\uparrow\downarrow} r_s^{\mathrm{W}} \tanh^2\left(\frac{t_{\mathrm{W}}}{2\lambda_s}\right)}{1 + 2G^R_{\uparrow\downarrow} r_s^{\mathrm{W}} \coth\left(\frac{t_{\mathrm{W}}}{\lambda_s}\right)}, \\
\frac{\Delta R_{\mathrm{AHE}}}{R} &= \theta_{\mathrm{SH}}^2 \frac{\lambda_s}{t_{\mathrm{W}}} \frac{2G^I_{\uparrow\downarrow} r_s^{\mathrm{W}} \tanh^2\left(\frac{t_{\mathrm{W}}}{2\lambda_s}\right)}{1 + 2G^I_{\uparrow\downarrow} r_s^{\mathrm{W}} \coth\left(\frac{t_{\mathrm{W}}}{\lambda_s}\right)}.
\end{aligned} \tag{3}$$

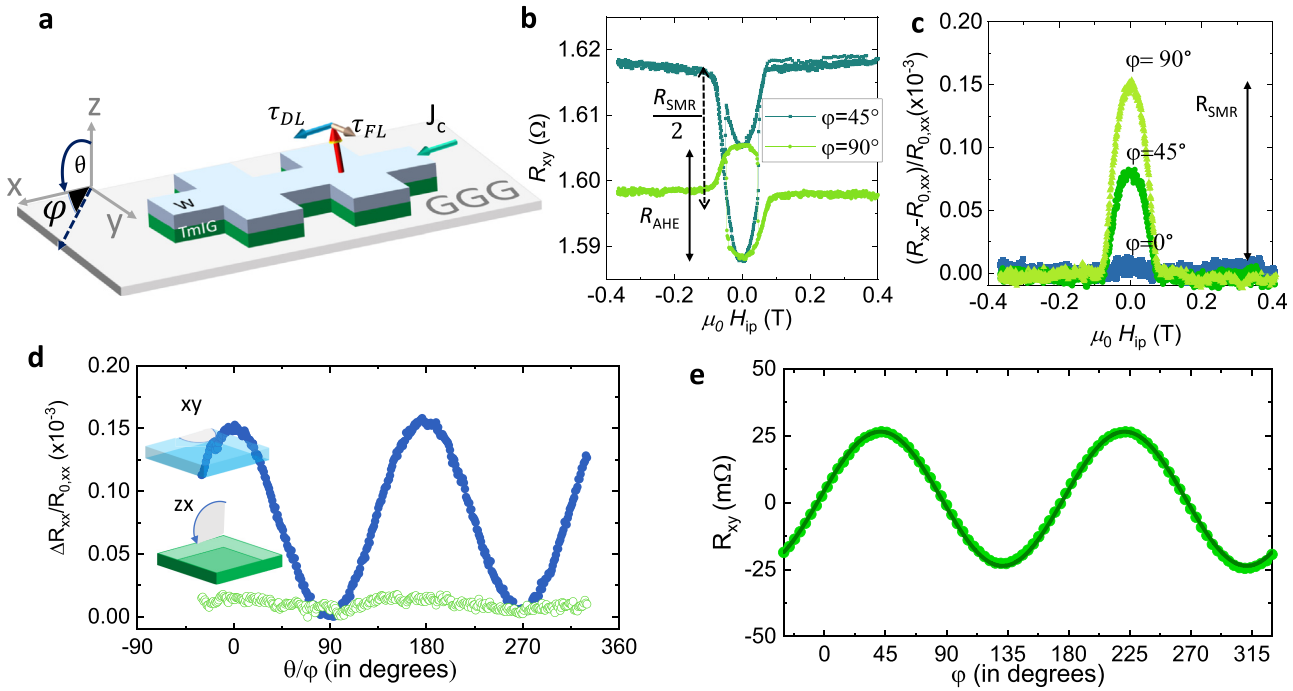

FIG. 2. (a) Schematic of the TmIG/W device on GGG. (b) Transverse (Hall) resistance (R_{xy}) as a function of the in-plane external magnetic field ($\mu_0 H_{\mathrm{ip}}$) at two azimuthal directions φ to quantify the SMR and AHE contributions. (c) Normalized longitudinal magneto-resistance, $\frac{\Delta R}{R_{0,xx}} = \frac{(R-R_{0,xx})}{R_{0,xx}}$ at different φ to disentangle the SMR and AMR. The value of $R_{0,xx}$ is 911 Ω. (d) Angle dependent $\frac{\Delta R_{xx}}{R_{0,xx}}$ in the xy- and zx-plane rotations. (e) Transverse (Hall) resistance (R_{xy}) as a function of the azimuthal angle (φ). The line is a fit according to Eq. (2).

From Eq. (2), $\theta = 90^\circ$ and $\varphi = 90^\circ$ gives our reference for the resistance R free of SMR and AHE. Thus, by varying θ, φ, one can quantify the two SMR/AHE contributions. Note that from Eq. (3), the SMR is scaled as θ_{SH}^2 leading to the independency upon of the sign of SHA [cf. Fig. 1(d)]. Now we focus on the variation in R_{xy} as a function of the magnetic field amplitude shown in Fig. 2(b), which is acquired at two different (φ) angles where the transverse SMR is maximum ($\varphi = 45^\circ$) and zero ($\varphi = 90^\circ$) according to Eq. (2).

In Fig. 2(b), we observe that the transverse SMR (R_{SMR}) and AHE (R_{AHE}) are simultaneously present. The (R_{SMR}) magnitude is estimated to be $\sim 2 \times 15 = 30$ mΩ (for the Hall crossbar of 5 μm width). Note that this value for W is significantly larger than the SMR observed on TmIG/Pt (6.5 mΩ)[12] with a ratio scaling with the corresponding spin Hall angle ratio. The occurrence of R_{SMR} and R_{AHE} stem concomitantly from the action of the respective SHE and inverse SHE (ISHE) in W following a spin-dependent reflection depending on the spin current absorption at the TmIG/HM interface. That way, R_{SMR} (R_{AHE}) is related to the real (imaginary) part of the interface spin-mixing conductance[19,29,30] [cf. Eq. (3)]. Furthermore, to identify the AMR contributions, the longitudinal resistance (R_{xx}) vs the in-plane magnetic field ($\mu_0 H_{ip}$) is shown in Fig. 2(c) for different angles φ. The absence of any resistance changes at $\varphi = 0^\circ$ definitely rules out the contributions from AMR in our sample. We also measured the angular dependence of R_{xx} within two different rotation planes, either *xy* or *xz*, as shown in Fig. 2(d). The resistance change within the *xy* rotation plane is fully consistent with the SMR observed in Fig. 2(c) giving the expected $\cos^2\varphi$ dependence. As previously shown in Fig. 2(c), the negligible change in resistance within the *zx* rotation plane seems to indicate the quasi-absence of any AMR-like signal, which may originate from proximity effects at the W interface.[31] It also indicates that the SMR is significantly larger in TmIG/W than in TmIG/Pt[12] owing to the large spin-Hall angle of W together with its larger resistivity. We also measured R_{xy} as a function of φ and verified that it follows Eq. (2) as shown in Fig. 2(e): the R_{SMR} is found to be $\simeq 28$ mΩ in agreement with the value obtained from the R_{xx} geometry [cf. Figs. 2(c) and 2(d)] owing to the form factor between the two types of measurements, which is $\Delta R_{xx}/\Delta R_{xy} \simeq 4.5$.

We now focus on the spin–orbit torque (SOT) properties in the TmIG/W bilayer using a second harmonic Hall analysis. The schematic in Fig. 2(a) depicts the vector components of SOTs acting on the magnetization of TmIG resulting from the absorption of the transverse components of the spin current at the TmIG/SHE material interface. The second harmonic Hall resistance measured at 0.12 T, within the in-plane magnetic field geometry, is displayed in Fig. 3(a). The injected

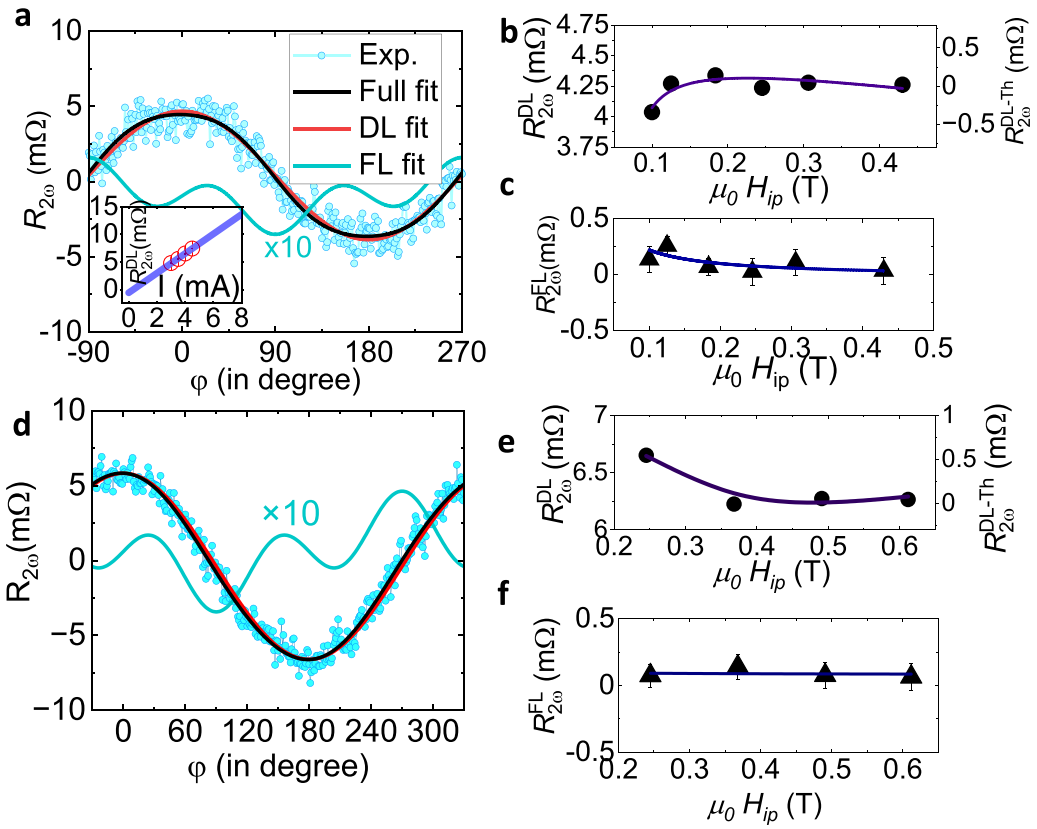

FIG. 3. (a) and (d) Second harmonic Hall resistance as a function of φ for TmIG/W(TmIG/Pt). Lines are fit to Eqs. (4)–(6). Note the factor of 10 between the cos φ variation and the cos 2φ sin φ variation. Inset (a): Damping-like second harmonic Hall resistance as a function of the ac-bias. (b) and (e) Damping-like (DL) and (c) and (f) field-like (FL) second harmonic resistances as a function of $\mu_0 H_{ip}$ to evaluate the DL and FL fields, respectively, for TmIG/W(TmIG/Pt). Lines are fit to Eqs. (5) and (6). During the second harmonic Hall resistance measurements, the current density in the W (Pt) was fixed to 1×10^{11} (2×10^{11}) A/m^2.

current was 3 mA corresponding to current density $J_c = 1 \times 10^{11}$ A/m^2 to record the signal at different in-plane magnetic fields. We can determine the DL and FL spin–orbit fields using the following relationships:[25,32,33]

$$R_{2\omega} = R_{2\omega}^{\mathrm{DL}} + R_{2\omega}^{\mathrm{FL}}, \tag{4}$$

$$R_{2\omega}^{\mathrm{DL}} = \left(\frac{R_{\mathrm{AHE}}}{2} \frac{H_{\mathrm{DL}}}{|H_{\mathrm{ip}} - H_k|} + R_{\mathrm{ANE/SSE}} + R_{\mathrm{ONE}} H_{\mathrm{ip}} \right) \cos\varphi, \tag{5}$$

$$R_{2\omega}^{\mathrm{FL}} = \frac{R_{\mathrm{PHE}}}{2} \frac{H_{\mathrm{FL}}}{|H_{\mathrm{ip}}|} \cos 2\varphi \sin 2\varphi. \tag{6}$$

Here, $\mu_0 H_{\mathrm{DL}}$ and $\mu_0 H_{\mathrm{FL}}$ are the current induced damping-like and field-like spin–orbit fields, respectively. These magnetic fields are responsible for the magnetization switching process.[34,35] $\mu_0 H_{ip}$ is the in-plane external magnetic field. $\mu_0 H_k$ is the anisotropy field and is estimated to be 52 mT. R_{SSE} is the resistance due to anomalous Nernst (ANE) or spin Seebeck effect (SSE) due to the thermal gradients produced by the Joule heating. R_{ONE} is the resistance due to the ordinary Nernst effect (ONE) scaled with the applied field. $R_{2\omega}$ is the second harmonic resistance as a function of the azimuthal angle (φ) shown in Fig. 3(a), which consist of both DL and FL contributions expressed in Eq. (4). The two terms are separately fitted along with the full fitting Eqs. (5) and (6). The values of $R_{2\omega}^{\mathrm{DL}}$ and $R_{2\omega}^{\mathrm{FL}}$ resistances are then used to calculate the two SOT fields $\mu_0 H_{\mathrm{DL}}$ and $\mu_0 H_{\mathrm{FL}} + \mu_0 H_{\mathrm{Oe}}$ employing Eqs. (5) and (6) as a separate fitting as shown in Figs. 3(b) and 3(c), respectively. $\mu_0 H_{\mathrm{DL}}$ and $\mu_0 H_{\mathrm{FL+Oe}}$ are found to equal -4.7 ± 1.6 and 1.14 ± 0.4 mT, respectively. The Ørsted field generated due to the applied current may be estimated from Ampère's law ($\mu_0 H_{\mathrm{Oe}} = J_c \times t_{\mathrm{W}}/2$). Using these values, we can estimate both DL and FL spin torque efficiencies,[36] $\theta_{\mathrm{SH}}^{\mathrm{DL(FL+Oe)}} = \frac{2e}{\hbar} \frac{H_{\mathrm{DL(FL+Oe)}}}{J_c} M_s t_{\mathrm{TmIG}}$ with resulting values equaling -0.14 ± 0.04 and 0.03 ± 0.01, respectively. Here, $M_s = 95$ kA/m and $t_{\mathrm{TmIG}} = 10$ nm are, respectively, magnetization and thickness of the TmIG layer. Similarly, we also measure the SOT efficiency in TmIG/Pt [see Figs. 3(d)–3(f)], and the magnitude of DL efficiency is found to be 0.05 ± 0.02, which is attributed to the larger spin Hall angle of W compared to Pt. The $R_{\mathrm{ANE/SSE}}$ and R_{ONE} are

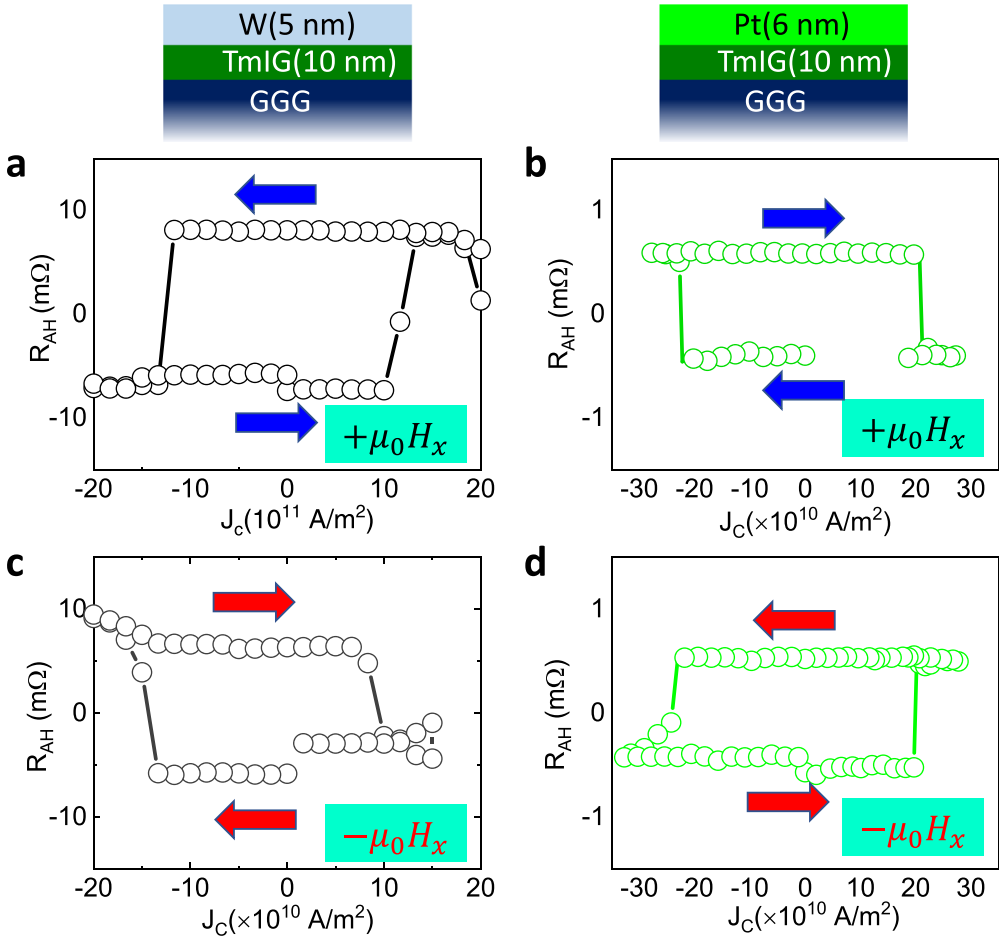

FIG. 4. (a) and (c) Magnetization switching at opposite magnetic fields. The switching polarity is counterclockwise (CCW) in $+\mu_0 H_x$ while CW with $-\mu_0 H_x$. The initial state is set to be $m_z > 0$ using the out-of-plane magnetic field of +0.35 T. (b) and (d) Current induced switching in the reference sample, TmIG/Pt. The current induced switching polarity is CCW in $-\mu_0 H_x$ while CW with $+\mu_0 H_x$, which is contrary to (a) and (c). The AHE signal also differs by more than one order of magnitude.

found to be $4.6 \pm 0.2\,\mathrm{m\Omega}$ ($-4.7 \pm 0.1\,\mathrm{m\Omega}$) and $0.8 \pm 0.2\,\mathrm{m\,\Omega/T}$ ($1.8 \pm 0.8\,\mathrm{m\Omega/T}$), respectively, for TmIG/W(TmIG/Pt). The thermal effects are removed and plotted on the right scale in Figs. 3(b) and 3(e). This indicates the significant contribution comes from the SSE with an opposite sign for W and Pt, which is expected in magnetic insulator/metal bilayer systems since the magnetic insulators are good thermally conducting materials.[37]

We now present the SOT (current pulsed) induced magnetization switching in the presence of a small in-plane magnetic field $\mu_0 H_x = \pm 4\,\mathrm{mT}$, which is applied parallel to the current. The results are shown in Fig. 4. The dc is injected in the range of 0–$\pm$8 mA (0 to $\pm 2.66 \times 10^{11}\,\mathrm{A/m^2}$). Since the hysteresis loop of the magnetization reversal induced by current pulses depends on the sign of the spin Hall angle, these measurements probe the sign of θ_{SH}. We clearly observe an inversion in the hysteresis loop when comparing W [Figs. 4(a) and 4(c)] and Pt [Figs. 4(b) and 4(d)]. The switching polarity is counterclockwise (CCW) for $\mu_0 H_x > 0$ while clockwise (CW) for $\mu_0 H_x < 0$ for W, whereas it is CW for $\mu_0 H_x > 0$ and CCW for $\mu_0 H_x < 0$ for Pt. It then demonstrates, as expected, that W and Pt have opposite spin Hall angle. We can also notice that, as explained by our evaluation of the torque in second harmonic measurement, the current density required to reverse the magnetization is reduced by a factor of nearly 2 in the case of the W layer. The amplitude of the AHE indicates that the magnetization is fully reversed in the Hall bar.

In summary, by analyzing the first and second harmonic longitudinal and transverse resistance in magnetic insulator/heavy metal systems with opposite spin Hall angle, we determined the origin of the anomalous Hall effect. The spin-polarized current absorbed through angular momentum transfer resulted in a resistivity change of the heavy metal known as the spin-Hall magneto-resistance, which is found to be responsible for the AHE-like signal. The observed AHE signal is independent of the sign of the spin Hall angle and follows its magnitude squared. Thus, our finding provides an understanding of the origin of the AHE in magnetic insulators in agreement with the theory of the spin-Hall magneto-resistance.[19]

The authors acknowledged the DARPA TEE Program Grant (MIPR No. HR0011831554) for their financial support. This work was supported by a public grant overseen by the French National Research Agency (ANR) as part of the "Investissements d'Avenir" program (Labex NanoSaclay, Reference No. ANR-10-LABX-0035).

AUTHOR DECLARATIONS

Conflict of Interest

The authors have no conflicts to disclose.

Author Contributions

Sajid Husain: Conceptualization (lead); Data curation (lead); Formal analysis (lead); Investigation (lead); Methodology (lead); Software (lead); Validation (lead); Visualization (lead); Writing – original draft (lead); Writing – review & editing (lead). **Nicholas Figueiredo Prestes:** Software (supporting); Visualization (supporting). **Olivier Fayet:** Visualization (supporting). **Sophie Collin:** Methodology (supporting). **Florian Godel:** Methodology (supporting). **Eric Jacquet:** Methodology (supporting). **Nicolas Reyren:** Formal analysis (supporting); Investigation (supporting); Validation (supporting); Visualization (supporting); Writing – review & editing (supporting). **Henri Jaffrès:** Conceptualization (supporting); Formal analysis (supporting); Funding acquisition (supporting); Investigation (supporting); Project administration (supporting); Resources (supporting); Supervision (supporting); Validation (supporting); Visualization (supporting); Writing – original draft (supporting); Writing – review & editing (supporting). **Jean-Marie George:** Conceptualization (equal); Data curation (equal); Formal analysis (equal); Funding acquisition (lead); Investigation (equal); Methodology (equal); Project administration (lead); Resources (lead); Supervision (lead); Validation (equal); Visualization (equal); Writing – original draft (supporting); Writing – review & editing (supporting).

DATA AVAILABILITY

The data that support the findings of this study are available from the corresponding authors upon reasonable request.

REFERENCES

[1]S. Takahashi and S. Maekawa, "Spin current, spin accumulation and spin Hall effect," Sci. Technol. Adv. Mater. **9**, 014105 (2008).
[2]A. V. Chumak, V. I. Vasyuchka, A. A. Serga, and B. Hillebrands, "Magnon spintronics," Nat. Phys. **11**, 453–461 (2015).
[3]T. Wimmer, M. Althammer, L. Liensberger, N. Vlietstra, S. Geprägs, M. Weiler, R. Gross, and H. Huebl, "Spin transport in a magnetic insulator with zero effective damping," Phys. Rev. Lett. **123**, 257201 (2019).
[4]K. Ichi Uchida, H. Adachi, Y. Kajiwara, S. Maekawa, and E. Saitoh, "Chapter one—Spin-wave spin current in magnetic insulators," in *Recent Advances in Magnetic Insulators—From Spintronics to Microwave Applications*, Solid State Physics Vol. 64, edited by M. Wu and A. Hoffmann (Academic Press, Cambridge, 2013), pp. 1–27.
[5]B. Dieny, I. L. Prejbeanu, K. Garello, P. Gambardella, P. Freitas, R. Lehndorff, W. Raberg, U. Ebels, S. O. Demokritov, J. Akerman *et al.*, "Opportunities and challenges for spintronics in the microelectronics industry," Nat. Electron. **3**, 446–459 (2020).
[6]Z. Guo, J. Yin, Y. Bai, D. Zhu, K. Shi, G. Wang, K. Cao, and W. Zhao, "Spintronics for energy-efficient computing: An overview and outlook," Proc. IEEE **109**, 1398–1417 (2021).
[7]A. Manchon, J. Železný, I. M. Miron, T. Jungwirth, J. Sinova, A. Thiaville, K. Garello, and P. Gambardella, "Current-induced spin-orbit torques in ferromagnetic and antiferromagnetic systems," Rev. Mod. Phys. **91**, 035004 (2019).
[8]J. Sinova, S. O. Valenzuela, J. Wunderlich, C. H. Back, and T. Jungwirth, "Spin Hall effects," Rev. Mod. Phys. **87**, 1213–1260 (2015).
[9]V. P. Amin and M. D. Stiles, "Spin transport at interfaces with spin-orbit coupling: Formalism," Phys. Rev. B **94**, 104419 (2016).
[10]V. P. Amin and M. D. Stiles, "Spin transport at interfaces with spin-orbit coupling: Phenomenology," Phys. Rev. B **94**, 104420 (2016).
[11]S. Vélez, J. Schaab, M. S. Wörnle, M. Müller, E. Gradauskaite, P. Welter, C. Gutgsell, C. Nistor, C. L. Degen, M. Trassin *et al.*, "High-speed domain wall racetracks in a magnetic insulator," Nat. Commun. **10**, 4750 (2019).
[12]C. O. Avci, A. Quindeau, C.-F. Pai, M. Mann, L. Caretta, A. S. Tang, M. C. Onbasli, C. A. Ross, and G. S. Beach, "Current-induced switching in a magnetic insulator," Nat. Mater. **16**, 309–314 (2017).
[13]H. Wu, S. A. Razavi, Q. Shao, X. Li, K. L. Wong, Y. Liu, G. Yin, and K. L. Wang, "Spin-orbit torque from a ferromagnetic metal," Phys. Rev. B **99**, 184403 (2019).
[14]Y. Yang, Z. Luo, H. Wu, Y. Xu, R.-W. Li, S. J. Pennycook, S. Zhang, and Y. Wu, "Anomalous Hall magnetoresistance in a ferromagnet," Nat. Commun. **9**, 2255 (2018).
[15]S. Ding, Z. Liang, C. Yun, R. Wu, M. Xue, Z. Lin, A. Ross, S. Becker, W. Yang, X. Ma, D. Chen, K. Sun, G. Jakob, M. Kläui, and J. Yang, "Anomalous Hall effect in magnetic insulator heterostructures: Contributions from spin-Hall and magnetic-proximity effects," Phys. Rev. B **104**, 224410 (2021).

[16]T. H. Dang, Q. Barbedienne, D. Q. To, E. Rongione, N. Reyren, F. Godel, S. Collin, J. M. George, and H. Jaffrès, "Anomalous Hall effect in $3d/5d$ multilayers mediated by interface scattering and nonlocal spin conductivity," Phys. Rev. B **102**, 144405 (2020).
[17]Q. Zhang, P. Li, Y. Wen, X. He, Y. Zhao, J. Zhang, and X. Zhang, "Interfacial scattering effect on anomalous Hall effect in Ni/Au multilayers," J. Phys. D: Appl. Phys. **50**, 235002 (2017).
[18]S. S.-L. Zhang and G. Vignale, "Nonlocal anomalous Hall effect," Phys. Rev. Lett. **116**, 136601 (2016).
[19]Y.-T. Chen, S. Takahashi, H. Nakayama, M. Althammer, S. T. B. Goennenwein, E. Saitoh, and G. E. W. Bauer, "Theory of spin Hall magnetoresistance," Phys. Rev. B **87**, 144411 (2013).
[20]C. O. Avci, A. Quindeau, M. Mann, C.-F. Pai, C. A. Ross, and G. S. D. Beach, "Spin transport in as-grown and annealed thulium iron garnet/platinum bilayers with perpendicular magnetic anisotropy," Phys. Rev. B **95**, 115428 (2017).
[21]Z. Luo, Q. Zhang, Y. Xu, Y. Yang, X. Zhang, and Y. Wu, "Spin-orbit torque in a single ferromagnetic layer induced by surface spin rotation," Phys. Rev. Appl. **11**, 064021 (2019).
[22]K. K. Vudya Sethu, S. Ghosh, S. Couet, J. Swerts, B. Sorée, J. D. Boeck, G. S. Kar, and K. Garello, "Optimization of tungsten β-phase window for spin-orbit-torque magnetic random-access memory," Phys. Rev. Appl. **16**, 064009 (2021).
[23]Y. Wang, P. Deorani, X. Qiu, J. H. Kwon, and H. Yang, "Determination of intrinsic spin Hall angle in Pt," Appl. Phys. Lett. **105**, 152412 (2014).
[24]Q. Shao, Y. Liu, G. Yu, S. K. Kim, X. Che, C. Tang, Q. L. He, Y. Tserkovnyak, J. Shi, and K. L. Wang, "Topological Hall effect at above room temperature in heterostructures composed of a magnetic insulator and a heavy metal," Nat. Electron. **2**, 182–186 (2019).
[25]Q. Shao, C. Tang, G. Yu, A. Navabi, H. Wu, C. He, J. Li, P. Upadhyaya, P. Zhang, S. A. Razavi *et al.*, "Role of dimensional crossover on spin-orbit torque efficiency in magnetic insulator thin films," Nat. Commun. **9**, 3612 (2018).
[26]C. Tang, P. Sellappan, Y. Liu, Y. Xu, J. E. Garay, and J. Shi, "Anomalous Hall hysteresis in $Tm_3Fe_5O_{12}$/Pt with strain-induced perpendicular magnetic anisotropy," Phys. Rev. B **94**, 140403 (2016).
[27]S. Husain, O. Fayet, N. F. Prestes, S. Collin, F. Godel, E. Jacquet, T. Denneulin, R. E. Dunin-Borkowski, A. Thiaville, M. Bibes, R. Nicolas, H. Jaffrès, A. Fert, and J.-M. George, "Field-free switching of perpendicular magnetization in an ultrathin epitaxial magnetic insulator," arXiv:2301.11469.
[28]X. Jia, K. Liu, K. Xia, and G. E. W. Bauer, "Spin transfer torque on magnetic insulators," Euro. Phys. Lett. **96**, 17005 (2011).
[29]H. Nakayama, M. Althammer, Y.-T. Chen, K. Uchida, Y. Kajiwara, D. Kikuchi, T. Ohtani, S. Geprägs, M. Opel, S. Takahashi, R. Gross, G. E. W. Bauer, S. T. B. Goennenwein, and E. Saitoh, "Spin Hall magnetoresistance induced by a nonequilibrium proximity effect," Phys. Rev. Lett. **110**, 206601 (2013).
[30]C. O. Avci, K. Garello, A. Ghosh, M. Gabureac, S. F. Alvarado, and P. Gambardella, "Unidirectional spin Hall magnetoresistance in ferromagnet/normal metal bilayers," Nat. Phys. **11**, 570–575 (2015).
[31]J. Sklenar, Y. Zhang, M. B. Jungfleisch, Y. Kim, Y. Xiao, G. J. MacDougall, M. J. Gilbert, A. Hoffmann, P. Schiffer, and N. Mason, "Proximity-induced anisotropic magnetoresistance in magnetized topological insulators," Appl. Phys. Lett. **118**, 232402 (2021).
[32]Q. Shao, G. Yu, Y.-W. Lan, Y. Shi, M.-Y. Li, C. Zheng, X. Zhu, L.-J. Li, P. K. Amiri, and K. L. Wang, "Strong Rashba-Edelstein effect-induced spin–orbit torques in monolayer transition metal dichalcogenide/ferromagnet bilayers," Nano Lett. **16**, 7514–7520 (2016).
[33]N. Roschewsky, E. S. Walker, P. Gowtham, S. Muschinske, F. Hellman, S. R. Bank, and S. Salahuddin, "Spin-orbit torque and Nernst effect in Bi-Sb/Co heterostructures," Phys. Rev. B **99**, 195103 (2019).
[34]K. X. Xie, W. W. Lin, H. C. Sun, Y. Nie, and H. Sang, "Time dependence of magnetization reversal influenced by current in perpendicularly magnetized Co/Pt thin film," J. Appl. Phys. **104**, 083907 (2008).
[35]W. W. Lin, H. Sang, D. Liu, Z. S. Jiang, A. Hu, X. S. Wu, and G. Xiao, "Magnetization switching induced by in-plane current with low density in pt/co/pt sandwich," J. Appl. Phys. **99**, 08G518 (2006).
[36]L. Liu, O. J. Lee, T. J. Gudmundsen, D. C. Ralph, and R. A. Buhrman, "Current-induced switching of perpendicularly magnetized magnetic layers using spin torque from the spin Hall effect," Phys. Rev. Lett. **109**, 096602 (2012).
[37]C. O. Avci, K. Garello, M. Gabureac, A. Ghosh, A. Fuhrer, S. F. Alvarado, and P. Gambardella, "Interplay of spin-orbit torque and thermoelectric effects in ferromagnet/normal-metal bilayers," Phys. Rev. B **90**, 224427 (2014).